# Fatty Acids Methyl Esters (FAME) autoxidation: 1 new insights on insoluble deposits formation process 2 in biofuels

M. Alves-Fortunato, E. Ayoub, K. Bacha, A. Mouret, C. Dalmazzone

# Fatty Acids Methyl Esters (FAME) autoxidation: new insights on insoluble deposits formation process in biofuels

*M. Alves-Fortunato*[1,*], *E. Ayoub*[1,2], *K. Bacha*[1], *A. Mouret*[2] *and C. Dalmazzone*[2]

[1]IFP Energies nouvelles, 1 et 4 avenue de Bois-Préau, 92852 Rueil-Malmaison, France ; Institut Carnot IFPEN Transports Energie, Combustion Systems and Fuels Department

[2] IFP Energies nouvelles, 1 et 4 avenue de Bois-Préau, 92852 Rueil-Malmaison, France, Physical-Chemistry and Complex Fluids Department

*E-mail : maira.fortunato@ifpen.fr

KEYWORDS: Autoxidation, biodiesel, methyl oleate, insoluble, deposits, FTIR, Turbiscan, phase separation rate, rapeseed methyl ester (RME), soy methyl ester (SME)

**ABSTRACT**

The thermal and oxidation stability of fatty acids methyl esters (FAME) is arousing attention in the transport industry, since they are the main components present in biodiesel products used in the market. Low FAME stability can induce easy fuel degradation and produce oxidation products that can form sticky deposits causing serious malfunctioning and failures of engine and turbines components. We have focused the present work on the study of fuel oxidation process and the characterization of oxidation products in order to identify the main levers to avoid deposits formation. Soy and Rapeseed biodiesels were oxidized using an autoclave Parr reactor and characterized by FTIR, density and viscosity measurements. After oxidation, two different liquid phases were clearly observed. These two phases tend to form complex oil-oil emulsions after remixing as evidenced by optical microscopy. The separation behavior of the different liquid phases remixed after oxidation were studied using Multiple Light Scattering (Turbiscan$^{TM}$). A comparison was made between the chemical functions of deposits obtained in the liquid phase after demixing (sedimented phase) and the solid deposits obtained on hot metallic surfaces. Results showed a that a complex oil-oil dispersion seems to form during the oxidation process. The phase separation rate of the oil-oil emulsified systems formed from oxidized fuels seems strongly related to the differences of polarity (e.g.oxygenates content) of both sedimented and supernatant phases. The understanding of this sedimentation or “demixing” process leading to deposits can be a key feature to develop strategies to prevent deposits formation in real systems.

**GRAPHIC ABSTRACT**

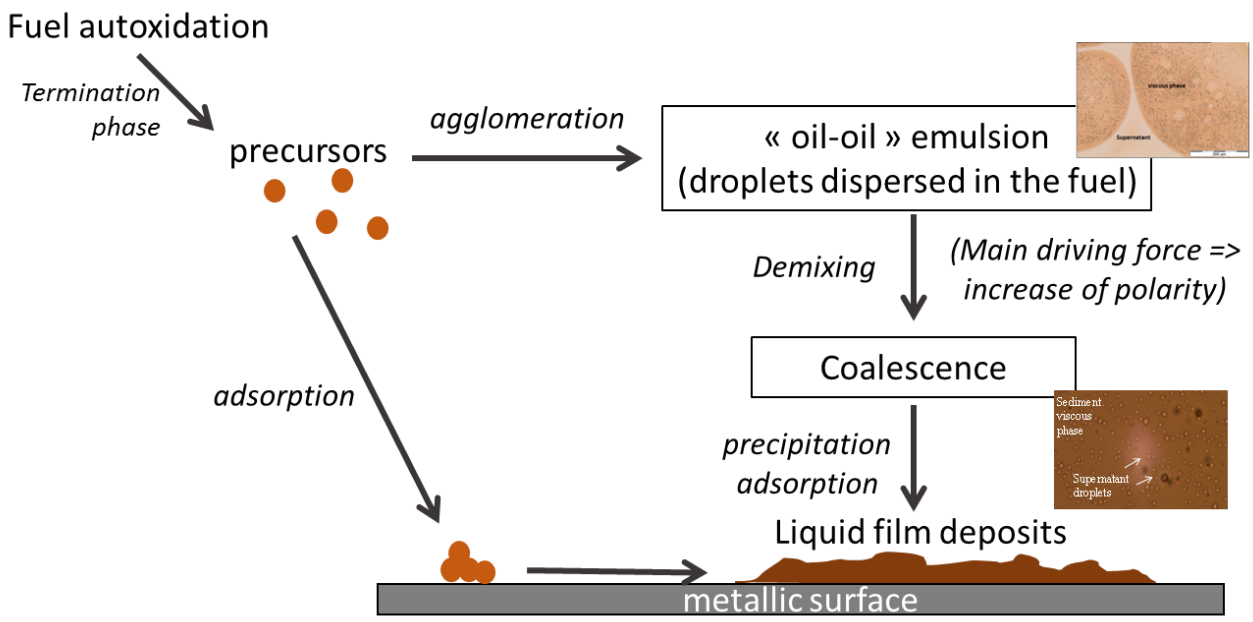


37

38

39 **HIGHLIGHTS**

40 • Oxidized fuel form an oil-oil complex emulsion

41 • Oxidized fossil diesel presents the most dense and viscous oxidation products, but it is
42 the slowest fuel to demix and to form deposits, i.e. products mass weight has a second
43 order impact on deposits formation

44 • The polarity of the oxidized fuel seems to play a major role in the liquid film deposits
45 formation

46

47

48

## 1. INTRODUCTION

Fatty acids methyl esters (FAME) autoxidation is involved in many complex processes in the healthcare and food industry (lipids deterioration issues)[1], transport industry (oxidation stability of biofuels)[2,3] and polymers applications (stability of polymers).[4] According to the literature, four main steps are involved in the autoxidation process based on the free radical chain reaction mechanism: primary initiation, secondary initiation, propagation and termination.[5,6] Primary and Secondary initiation correspond to the formation of free radicals by temperature, catalysis by metals,[7] and/or natural hydroperoxides impact over hydrocarbons chains.[1] These free radicals are highly reactive generating chain reactions producing more radicals accelerating the degradation process. The last step (termination) corresponds to the formation of stable products (e.g. polymers, dimers, epoxides, aldehydes, cyclic peroxides,…). The autoxidation stable products are pointed out as one of the main causes of the formation of insoluble in the liquid phase.

Depending on the oxidation level, different phases can be visually observed in the sample. A light brown to dark brown dense phase can be identified in the bottom of the flask or in the system in contact with the fuel.[8] This insoluble phase is sticky and may be at the origin of the deposits observed in real engines/turbines systems. This kind of deposit correspond to the "lacquer" and/or "sticky" deposit as proposed by Baker *et al.[9],* these deposits are very viscous and quite adherent to the surface, they are difficult to remove even when using solvents such as acetone. According to the author, this category of deposits is directly linked to polymeric films and aged fuels. According to Fang et McCornick,[10] autoxidation products could be kept in suspension into the liquid phase fuel depending on their polarity and/or molecular weight as well as the interaction with the solvent. Our last work[11] on oxidation process of biofuel surrogate

(methyl oleate/*n*-dodecane) has shown that during oxidation small aggregates are formed, fuel color changes and phase separation occurs when the number of clusters in the liquid phase is higher than 10 and with a molecular weight larger than 3500 g/mol, the aggregates sizes increases linearly with the number of particles and, at the same time, oxygenate products epoxides and ketones can be identified, they could certainly increase the polarity of the sample. The deposits observed in injector systems would be formed when the polarity and/or the molecular weight of the autoxidation production in suspension are sufficiently high, inducing precipitation of polymeric deposits. Bacha *et al.*[12] have shown that the chemical composition of aged biofuels is mainly composed of oxygenated products, as expected, and the molecular weights of these products are higher than the fuel initial products. Other authors have also pointed out the more oxygenated nature of autoxidation products which is inherent to free radical chain reaction mechanism. Nevertheless, to the best of our knowledge, no systematic study was performed to identify which parameter between polarity and molecular weight, could lead to insoluble deposition. This is an important point that must be addressed in order to properly frame the problem and to focus efforts to strategically prevent and avoid the deposition phenomena and help in the development of more adapted fuel additives, improved fuel formulations or in the design of specific coatings for surfaces in contact with fuels.

Here we have studied the fuel oxidation process and the characterization of oxidation products, especially the oil-oil complex system formed after oxidation which separates, leading to a supernatant phase and a sedimented phase, which is likely to adhere on a metallic surface leading to deposits. Soy Methyl ester (SME) and Rapeseed methyl ester (RME) biodiesel feedstock and Diesel (B0) as well as their blends were studied and characterized by FTIR, density and viscosity measurements. Also, the emulsion formed after mixing of the separated

liquid phases obtained after oxidation was studied, in particular the phase separation process. Deposits were formed on a hot metallic surface in the laboratory conditions using a microcoking device. A comparison was made between the chemical functions of deposits obtained in the liquid phase and the deposits obtained on metallic surfaces.

## 2. EXPERIMENTAL METHODS

### 2.1 Fuel Matrix

The fuel reference used was the B0 diesel fuel which is a commercial diesel fuel matching the European Automotive Diesel fuel specification EN590 supplied by Analytic Service Gesellschaft (ASG). The B0 is free from fatty acid methyl esters (FAME). The chemical analysis is presented in Appendix. The FAME feedstocks studied were Rapeseed Methyl Ester (RME) and Soybean Methyl Ester (SME), both fuels do not contain antioxidant additives and were supplied by ASG. Table 1 presents the different samples obtained from diesel/biodiesel blends. In addition to real fuels, methyl oleate was studied as a biodiesel surrogate. Methyl oleate is the main component of RME biodiesel (chemical analysis is provided in the Appendix).

**Table 1. Fuel Matrix used in the present study: fuel notation and blends composition.**

| **Fuel notation** | **Composition** |
|---|---|
| B0 | Diesel EN590 |
| B10RME | B0 + 10%v/v RME |
| B10SME | B0 + 10%v/v SME |

| | |
|---|---|
| B30RME | B0 + 30%v/v RME |
| B30SME | B0 + 30%v/v SME |

111

112 **2.2 Fuels oxidation**

113 To study fuels oxidation we have used an accelerated oxidation method based on an in-house
114 autoclave reactor. Some standard methods use the principle of accelerated oxidation tests such as
115 the Rancimat (EN 15751) or the Rapid Small Scale Oxidation Test (RSSOT) also known as
116 PetroOxy test (ASTM D7525 – for gasoline, ASTM D7545 – for diesel and biodiesel). In our
117 case, we use an in-house method derived from the PetroOxy method. The autoclave reproduces
118 the same air/fuel ratio as the PetroOxy test, but with the advantage to allow samplings during the
119 test. With this method we are able to follow not only the pressure drop, as in the PetroOxy
120 method, but also the chemical species that are formed during the process (the detailed
121 methodology is given elsewhere [13]).

122 The autoclave *Parr* (Figure 1) was filled with 50mL of (bio)fuel. The air was removed from the
123 cell by flushing Helium. Then, the temperature was raised under inert conditions until the desired
124 temperature. Once the temperature of the test is reached, the Air is introduced in the cell,
125 replacing the inert gas. Experiments were performed at isothermal condition at 150°C during 5
126 hours. The fuel was maintained under constant stirring to achieve homogenous temperature
127 inside the reactor chamber. The pressure variation was monitored in order to ensure a constant
128 air pressure of 7 bars and to avoid diffusional limitations of the autoxidation process (further set
129 up information elsewhere)[13].

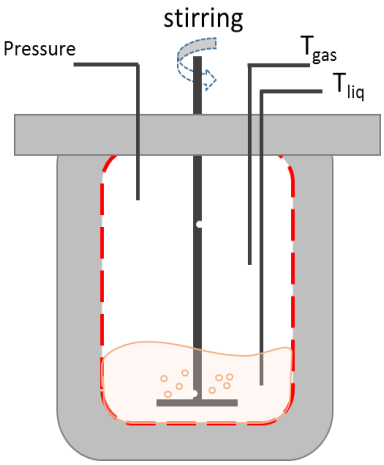


**Figure 1. Schema of autoclave Parr[13].**

After 5 hours, the oxidized fuels presented a phase separation, with two different liquid phases here named “supernatant phase” and “sediment phase”, as it is shown in figure 2:

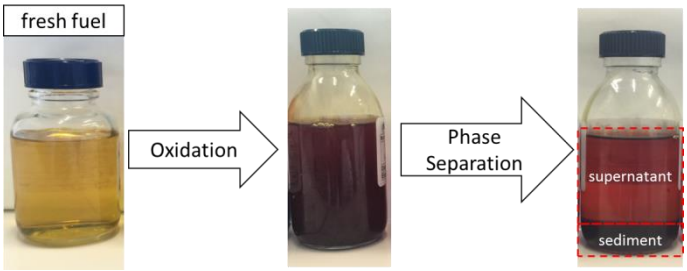


**Figure 2. Photo of fuel before and after oxidation as well as the indication of supernatant and sediment phases observed after phase separation**

It is important to highlight that accelerated methods as Autoclave, RSSOT and Rancimat have already been studied in the literature by comparing their deposits with the fuel “insoluble” phase observed during storage and/or into fuel injection systems. [14–16] The deposits obtained with these methods can be compared to the ones in real systems.

### 2.3 Characterization

144 The density was measured with an Anton Paar densimeter, (DMA4500M) at 15°C. The viscosity
145 was determined at 20°C with a TA Instruments Rheometer, (DHR3), equipped with double air
146 gap coaxial cylinders for low viscosities (supernatant phase) and a cone plate geometry (4 cm
147 diameter and angle of 2°) for higher viscosities (sedimented phase).

148 Optical microscope BX51 (OLYMPUS), with 100x image enhancement, was used to observe
149 objects formed into each phase of oxidized samples. The lower limit of the technique is 1$\mu$m.

150 The Turbiscan™ apparatus (Classic MA2000) was used to analyze the separation rate of the
151 different phases obtained after fuel oxidation after re homogenization (by hand shaking). This
152 technique called Multiple Light Scattering (MLS) consists in sending photons (light) into the
153 sample. These photons, after being scattered many times by objects in suspension (droplets, solid
154 particles, gas bubbles, …) emerge from the sample and are detected as a function of time by the
155 sensors (transmission and backscattering). A mobile reading head, composed of a NIR diode and
156 two detectors, scans a glass cell containing the sample. The decrease of the transmission signal
157 indicates the formation of particulates or droplets. The measurements were performed after
158 sample homogenization so that the droplets formed are homogeneously dispersed. The results are
159 given in terms of percentage of transmission as a function of the height of liquid in the tube for
160 different times. . More details about Turbiscan™ analysis are presented elsewhere [17,18].

161 The global chemical composition of the fuel was evaluated by mid-IR. FTIR spectra were
162 recorded using a horizontal ATR cell, with ATR diamond mono reflection (Golden Gate),
163 covering 600-4000 $cm^{-1}$ spectral range. Each FTIR-ATR spectrum is in the average of 100 scans
164 using air as reference at a resolution of 4 $cm^{-1}$, and all spectra were collected at ambient
165 temperature.

A microcoking device was used to evaluate the tendency of the fuel to form deposits when heated (thermal stability). Originally it is a standard method “GFC-Lu-27” to evaluate lubricants degradation. The method was adapted in order to be compatible with fuels analysis. Figure 3 shows the schema of the apparatus. It consists of a metallic plate, in our case made of stainless steel, heated by two heating blocks where the temperature is controlled by two thermocouples and maintained at 150°C, this temperature was chosen since it is representative of real injector temperature range in the engines. 4mL of fuel were placed using a syringe in the hollow of the stainless steel plate. The time to visually observe a lacquer formation was evaluated as well as the chemical functions of the deposits formed on the plate.

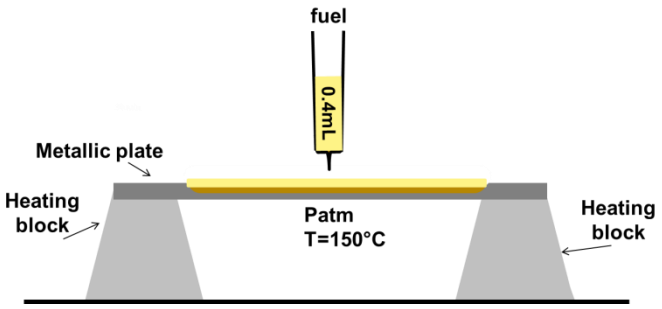


**Figure 3. Microcoking device. The metallic plate is made of stainless steel.**

It is noteworthy that the operation condition of the microcoking device favors the evaporation of higher volatile compounds and the oxidation of the “heavier” compounds that remain in contact with the hot metallic surface. In the case of FAMEs, Bacha [19] have studied and compared the deposits formed into the reactor and the ones formed with the microcoking device. The results obtained with FTIR and thermogravimetric analysis (TGA/DTA) have shown that the deposits obtained with PetroOxy and microcoking device are very similar presenting the same chemical functions at FTIR and the same profile of the thermogravimetric analysis.

## 3. RESULTS

Aged fuels presented a diphasic complex system that after remixing gives a complex emulsion as observed by optical microscopy (Figure 4). Two main phases can be identified: Figure 4-left presents the emulsion after homogeneization by hand shaking of the liquid phases obtained after oxidation. The shaking method was used to achieve a soft and reproducible homogenization of phases, the measurement was made during 10 seconds for each sample, it was repeated two times and it is reproducible. Figure 4-right presents the sediment phase of the emulsion after phase separation or demixing. The phase separation is achieved under the only action of gravity in order to observe the process as it occurs naturally in real systems.

The images of fresh fuels obtained from optical microscope do not show any droplets or particles (not shown here). On the other hand, images from the fuel after oxidation (Figure 4-left) present an interesting complex non-homogeneous emulsion formed by supernatant droplets into sediment droplets and vice-versa for all fuels, including B0 (fossil diesel biodiesel-free). These droplets are not homogeneous in shape or size. In addition, no feature or tendency has been observed to link the droplets size to biodiesel feedstock or phase separation rate. After demixing, the supernatant phase does not present any dispersed particles or droplets (not shown here). The sediment phase presents a continuous viscous area with small droplets of supernatant phase dispersed into it (Figure 4-right).

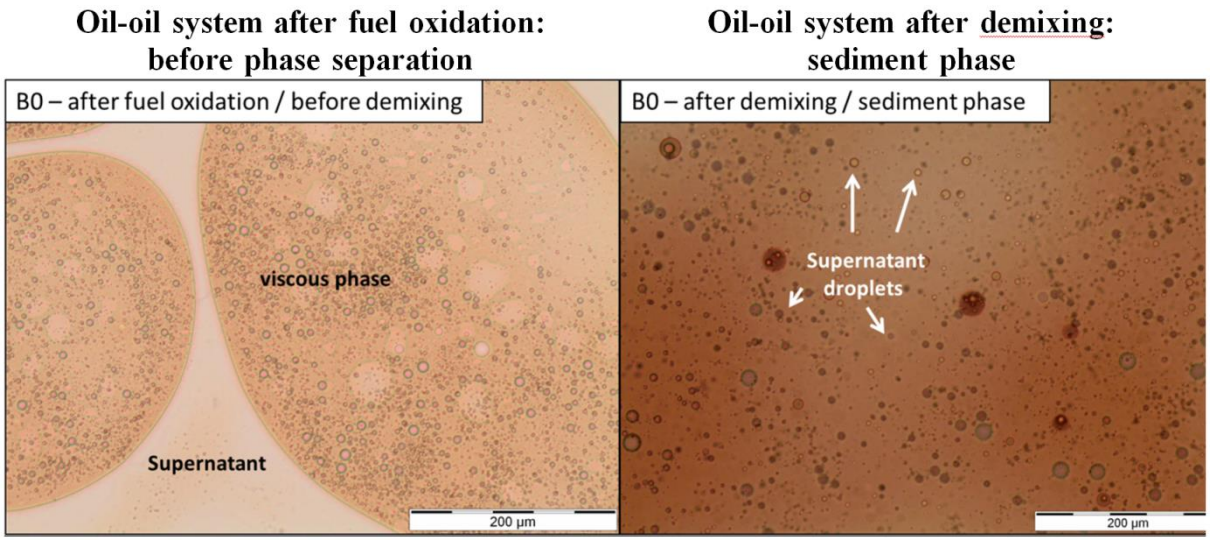


204

205 **Figure 4. Optical microscopic images of oxidized B0 before (left) and the sediment phase (right) after demixing.**

206

207 The viscosity of fresh fuels as well as the supernatant and sediment phases after oxidation of all

208 fuels is presented in Figure 5.

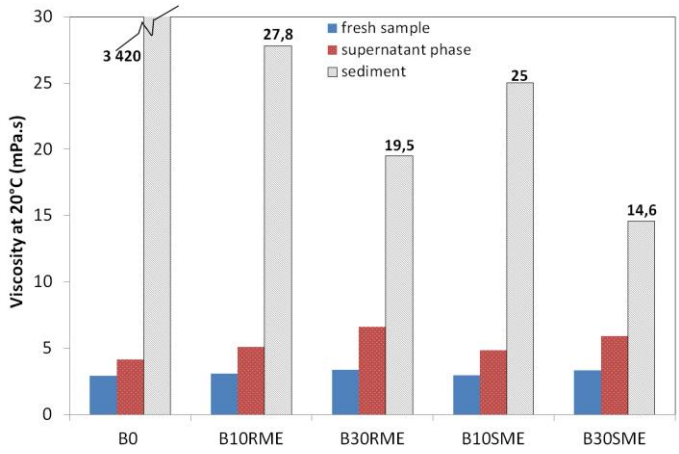


209

210 **Figure 5. Viscosity of fresh fuels (blue), supernatant phase (red) and sediment phase (grey)**

211

212 The viscosity of the supernatant phase presents a slightly higher value than the one of the

213 corresponding fresh fuels. The difference is around 30% for B0, 38% for B10SME and B10RME

and achieving almost 50% for B30 RME and SME samples in comparison to fresh fuel samples. For the sediment phase, the viscosity values are around 5 times higher for B10 samples and 2.5 to 3 time higher for B30 samples than the viscosity of fresh fuels. The main difference between sediment phase and fresh fuel viscosity is observed in the case of B0 for which it was more than 800 times higher. Considering the viscosity of the sediment phases, the ranking for the different fuels is B30SME < B30 RME < B10SME < B10RME <<< B0.

Figure 6 shows the density results. The differences between the sediment and supernatant phases are less marked than for the viscosity results previously presented. The sediment phase density is only 1.0 to 1.5 times higher than the one of corresponding fresh fuels, including B0. The ranking obtained is almost the same as before: B30SME ~ B30 RME < B10SME ~ B10RME < B0. It is noteworthy that fuels containing the same amount of biodiesel have similar densities, independently from the feedstock.

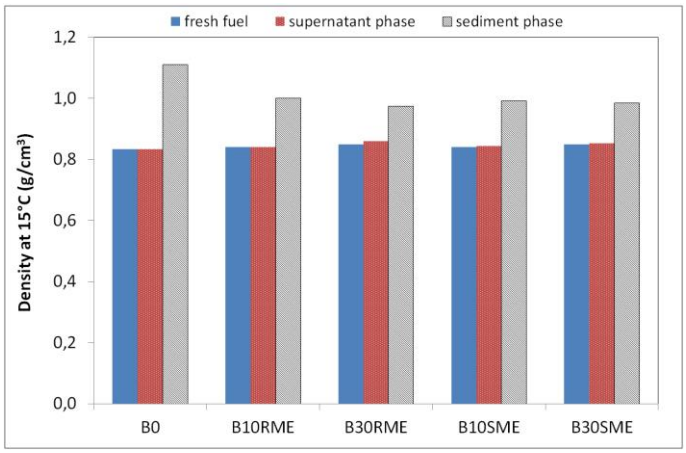


**Figure 6. Density of fresh fuels (blue), supernatant phase (red) and sediment phase (grey)**

### 3.1 Phase separation after rehomogeneization of aged fuels

Based on the previous results one can wonder if the demixing process is directly related to the increase of viscosity and density observed for oxidized fuels (hence related to the molecular weight of the products). Turbiscan was used to determine the demixing rate of all rehomogenized fuels. The test tubes were filled with aged fuels. Table 2 gives the initial respective heights of supernatant and sediment phases.

**Table 2. Heights of sediment and supernatant phases in the Turbiscan test tube**

| Aged fuel | Sediment Phase (mm) | Supernatant Phase (mm) | Ratio (%) (sediment/supernatant) |
|---|---|---|---|
| B0 | 3 | 70 | 4 |
| B10 SME | 8 | 67 | 12 |
| B10 RME | 6 | 65 | 9 |
| B30 SME | 8 | 65 | 12 |
| B30 RME | 4 | 71 | 6 |

Figures 7a-e show the transmission signal profile of the fuels as a function of the test tube height at different times. Initially, the transmission signal is close to zero all along the tube. Then, phases begin to separate into a supernatant and sediment phases. This process of separation can be quite long, as in the case of B0 for which even after 170h, the transmission signal is not completely flat in the supernatant phase. At short times, it is noteworthy that the fastest demixing rate is obtained for B30 SME (more than 20% of transmission in the supernatant at 10 min) and

the lowest with B0 (less than 10% at 10 min), the behavior of the other fuels being very similar. At longer times, the differences between the aged biofuels is less pronounced.

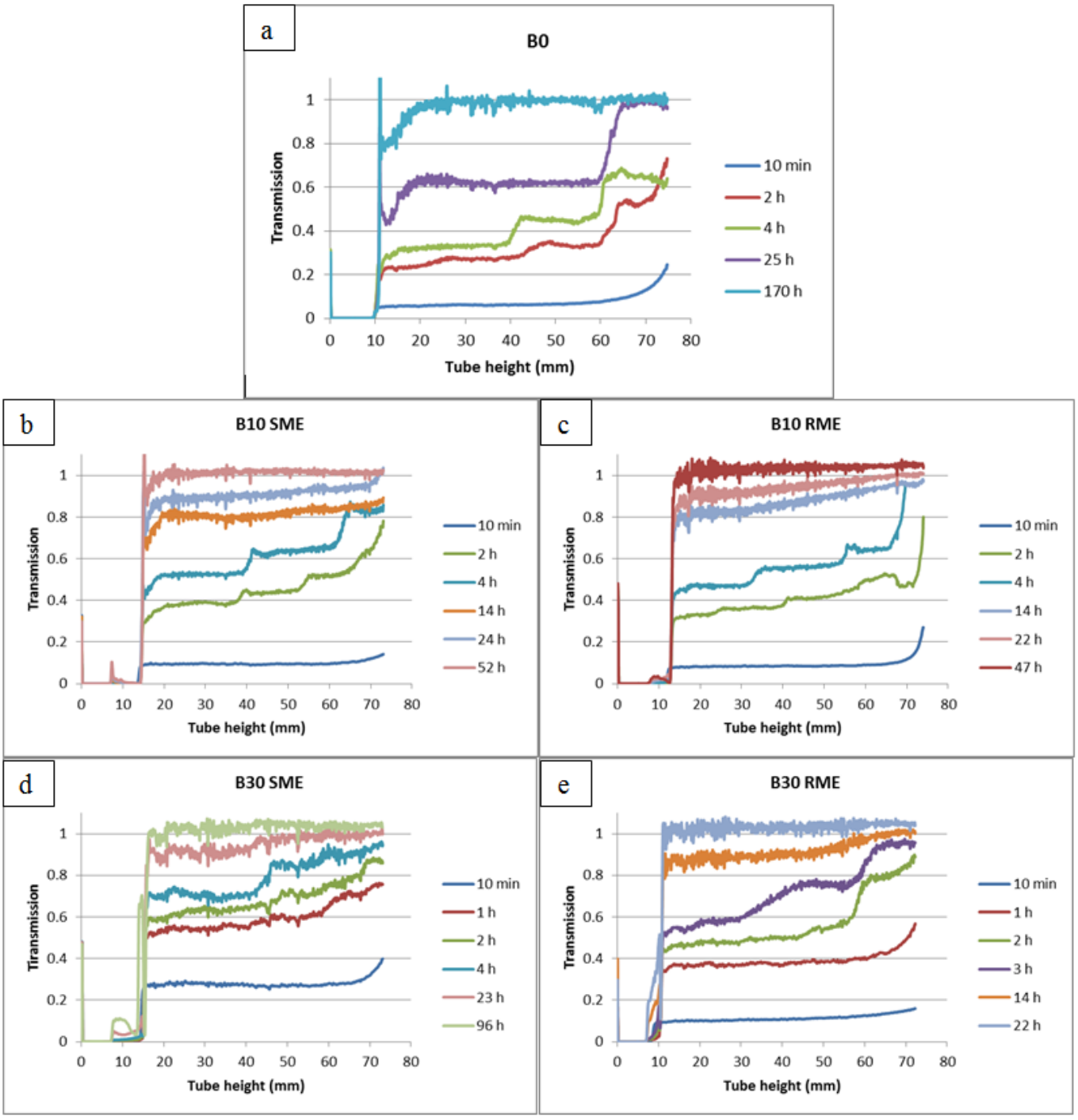


**Figure 7a-e. Turbiscan results - Evolution of the transmission signal versus test tube height at different times for different aged fuels: a) B0, b) B10 SME, c) B10 RME, d) B30 SME, e) B30 RME (0: no transmission – 1: 100% of transmission)**

The evolution of the transmission signal in the middle of the test tube was plotted for each aged fuel as a function of time in Figure 8. These results confirm that aged biofuels exhibit similar separation rates, i.e. they seem to be fairly good surfactants and so favoring the demixing process. B10 and B30 samples achieve more than 60% Transmission after only 5h, achieving 100% Transmission in less than 25 h for the B30 fuels and 45 h for the B10. It means that the phases are completely separated. On the other hand, B0 is characterized by a very low demixing process compared to the others, it does not achieve 100% Transmission even after two days testing.

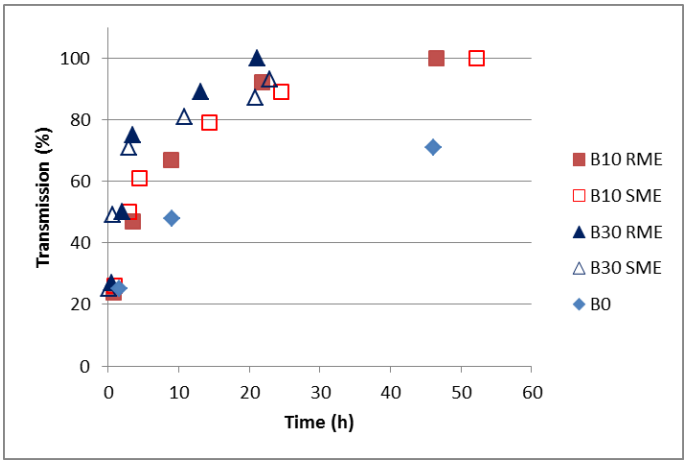


**Figure 8. Turbiscan results: time to achieve different level of the transmission signal in the middle of the test tube for B0, B10RME, B30RME, B10 SME and B30SME.**

Thus, the ranking for the phase separation rate is B0<<< B10RME~B10SME~B30RME ~B30SME, with B30 samples being the fastest ones to present the viscous sediment phase observed in oxidized samples. It is noteworthy that this ranking is completely the opposite of the

one obtained previously for density and viscosity. It indicates that the fuel presenting the highest dense and viscous sediment phase is not the first one to achieve phase separation.

The observation confirms the hypothesis that some oxidation products seem to remain quite stable dispersed in the oil-oil system which could cause the slow phase separation rate of the sample. In order to understand what causes the stability of some oxidation products in the emulsion, an infrared spectroscopy was carried out for the fresh system before oxidation , for both supernatant and sediment phases, after oxidation (phase separation) as well as for the deposits formed using the microcoking device as described in the experimental section.

### 3.2 Aged fuels and deposits infrared spectroscopy characterization

The FTIR spectra profiles of B0, B10RME and B30RME are presented on Figure 9, 10 and 11 respectively. The results named "deposit" corresponds to the FTIR spectra of deposits generated over the stainless steel surface. For all fuel two main regions of the spectra can be distinguished: the one around 3600-3000$cm^{-1}$ corresponding to –OH band and the region around 1770-1710$cm^{-1}$ linked to –C=O vibration. In all fresh fuels these regions are flat, no band intensity is detected. However, these regions are prominent for all the aged fuels as well as the deposits over stainless steel .

Fresh B0 diesel spectra (Figure 9) does not present any oxygenate chemical function. On the other hand, B0 oxidized samples (supernatant, sediment and deposit) present a very broad band corresponding to -OH at 3600-3000$cm^{-1}$ as well as a large band at 1730-1725$cm^{-1}$ and a sharper band centered at 1715-1710$cm^{-1}$ which may correspond to ketones, aldehydes and carboxylic acid chemical functions, the latest being in agreement with the –OH presence. In addition, the

deposit presents a broad band at 1772 $cm^{-1}$ which could be assigned to anhydrides acids. This band is much less marked on the supernatant and sediment phases. It is worth mentioning that there is no marked difference between supernatant and sediment phase. The chemical functions of B0 supernatant and sediment phases are the same, i.e. new chemical groups do not emerge in the sediment spectra in comparison to supernatant spectra, this can indicate that the B0 degradation products can remain relatively stable in suspension which is in agreement with Turbiscan$^{TM}$ results.

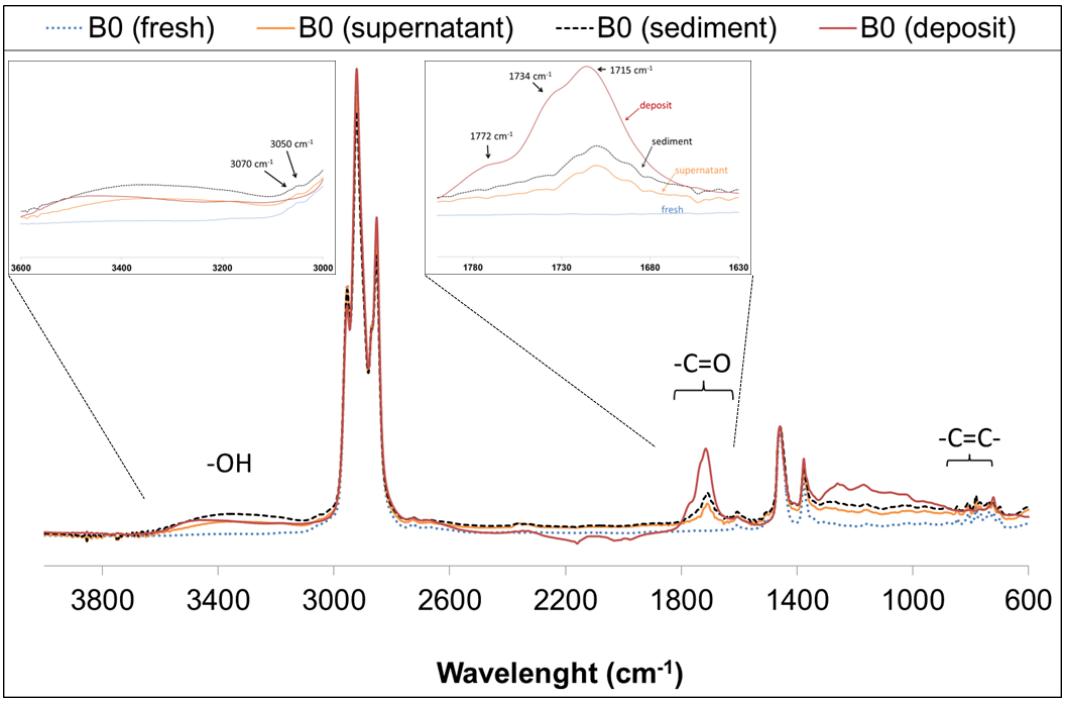


**Figure 9. FTIR spectra of B0 fresh (dot blue) , aged fuel after demixing supernatant (orange) and sediment phase (dash dark) as well as the deposit formed over the stainless steel (red line) surface using the microcoking device**

It is interesting to notice the difference between the deposit and the sediment spectra. As already mentioned, the chemical functions are mainly the same, but the broad band assigned to –OH function and the band at 1772$cm^{-1}$, that could correspond to anhydrides, are different in both

samples. The –OH is less marked in the deposits whereas the 1772cm$^{-1}$ band is less marked in the sediment. One of the mechanisms to anhydrides formation is the dehydration of carboxylic acids: 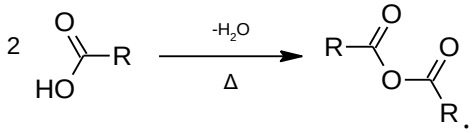 . The species involved in this reaction mechanism would be in agreement with the observation of the less marked –OH bands in the deposits than in the sediment and, on the other hand, the appearance of the 1772 cm$^{-1}$ band in the deposit spectra. This type of reaction can occurs at T > 100 °C without catalyst which means that the stainless steel surface would probably have no impact on the deposits formation, i.e. no catalytic effect. This hypothesis will be further investigated in a future work.

In the case of biodiesel fuels, the differences between supernatant and sediment phases are clear (Figure 10 and Figure 11). A large band at 3600-3000cm$^{-1}$ is observed for both fuels in the sediment phase which corresponds to -OH chemical function. Also, the band at ~1711cm$^{-1}$ is intense in the sediment, indicating the formation of compounds containing aldehydes, ketones, and/or carboxylic acids chemical functions. The same trend is obtained for the bands at 1436cm$^{-1}$ and 1378cm$^{-1}$, corresponding to vibrations –C-OH bending (for carboxylic acids) or α-$CH_2$ bending (for ketones) [20][21].

Thus, as expected, oxygenate chemical groups onset can be observed for B10 and B30 fuels as for B0. The main difference is that for B0 the supernatant phase and the sediment phase do not present a marked different in both spectra, i.e. they present very similar chemical functions, which could indicate that there is very little polarity contrast between supernatant and sediment phases for the B0 Diesel fuel. On the other hand, for B10RME and B30RME there is a clear difference between sediment phase and supernatant phase for both -OH region and -C=O region.

For these fuels, the supernatant phase is similar to the fresh fuel, especially for the -OH region, whereas the sediment present a remarkably higher ratio of oxygenates (considering the hydroxy and carbonyl groups). The B10RME deposits over stainless steel present the same chemical profile as the oxidized fuel, no new chemical function is observed in the deposits in comparison to the sediment phase. Nevertheless, a dimeric -OH stretch can be distinguished for the B30RME deposit, at 3505cm$^{-1}$ and 3466cm$^{-1}$ which is not present on liquid samples.

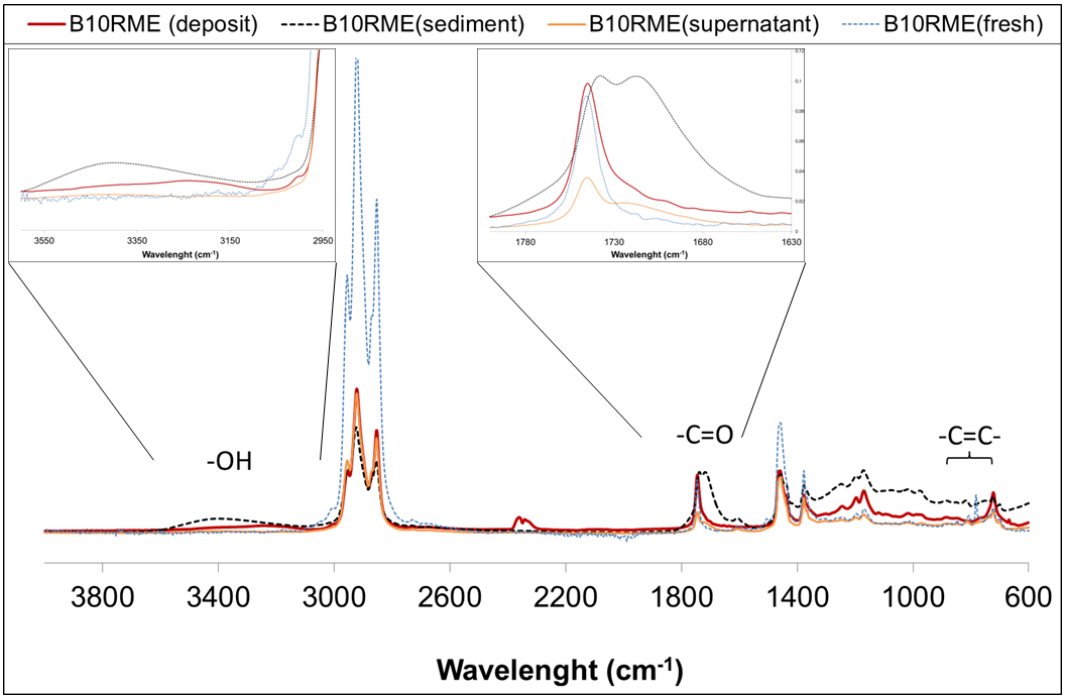


**Figure 10. FTIR spectra of B10RME fresh (dot blue) , aged fuel after demixing supernatant (orange) and sediment phase (dash dark) as well as the deposit formed over the stainless steel (red line) surface using the microcoking device**

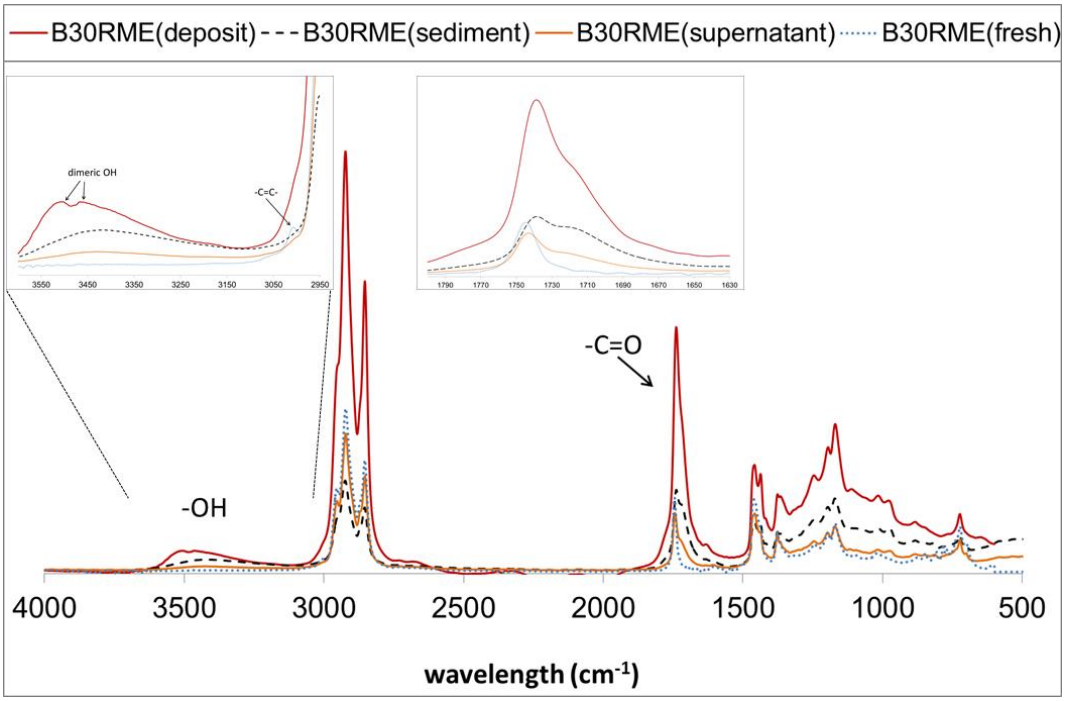


**Figure 11. FTIR spectra of B0 (A), B10RME (B) and B30RME (C) of: fresh samples (blue), supernatant phase (red), sediment phase (black) and deposit over stainless steel surface**

It is noteworthy that the deposit spectra for both biodiesel samples do not present the band assigned to the anhydride that was present in the B0 sample. In addition, beyond its presence, the dimeric –OH band in the deposit seems to be more intense in comparison to the B0 sample.

## 4. DISCUSSION

The free radical mechanism is the most accepted and studied pathway to fuels autoxidation. It includes mainly three main steps: initiation, propagation and termination [1,22–24]. Initiation corresponds to free radicals formation by temperature, catalysis by metals, and natural hydroperoxides (ROOH) impact over FAME molecule (RH). Schaich [6] has studied different

pathways involving not only hydrogen abstraction, which is the most studied pathway, but also internal cyclization, addition, scission, and disproportionation reactions. According to the author these pathways are competitive or even dominant under some conditions, leading to variations in oxidation kinetics and, in particular, the final products obtained. The free radicals formed, which are highly reactive, generate branching chain reactions producing more radicals causing fast degradation (propagation phase). Radicals chain reactions slow down when more stable products (e.g. polymers, epoxides, aldehydes, cyclic peroxides,…) start to be formed (termination phase). Deposits observed on fuel systems are formed from these stable oxidation products. FAME molecules structure (especially the terminal carboxyl and unsaturation level) impacts the reactivity and the stable products that are formed during autoxidation process. Several routes can be considered during the initiation and propagation process.

Here, stable oxidation products onset are observed in oxidized fuels as indicated by the different chemical functional groups of FTIR analysis. The formation of these products may correspond to the termination phase [1,25,26]. (see Figure 12). Once the termination process starts with the formation of stable products, which are the deposits precursors, a liquid phase separation can be observed leading to a dense viscous phase in the bottom and a supernatant phase.

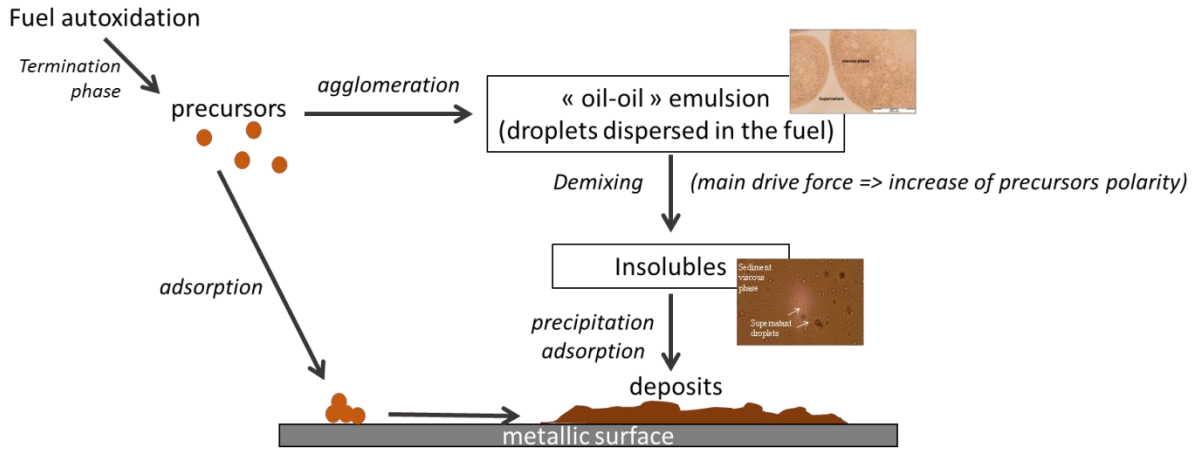


**Figure 12. Schema of the deposits formation mechanism proposed**

Optical microscopy performed on oxidized fuels after rehomogenization shows that a complex oil-oil system emulsion is formed, with the presence of small droplets dispersed in the fuel. These dispersed objects go through a precipitation process. The "demixing" rate of B30SME is much faster than B0 diesel as observed by Turbiscan measurements. The "demixing" of B10SME, B10RME and B30RME are very similar but faster than B0 diesel as well. The separation of the oxygenate compounds from the fuel phase is not directly linked to the difference of density and viscosity of these products since Turbiscan results present the opposite ranking. Indeed density and viscosity results have shown much higher values for B0 diesel than for the other samples. It means that the fastest fuel to produce deposits is not the one with the most dense or viscous sediment phase. **There is no straightforward link between the molecular weight of particulates and the deposits observed.**

**Therefore, the difference of polarity between particulates formed by oxygenates species and the fuel seems to be the main driving force of deposits precipitation after fuel degradation.**

By analyzing both phases, supernatant and sediment, formed after particulates precipitation by FTIR, it seems that the particulate objects are mainly composed of oxygenate molecules as carboxylic acids, alcohols, aldehydes, esters and ketones. These oxygenate species correspond to the chemical functions observed at deposits over stainless steel.

The presence of same type of oxygenated chemical functions in the sediment phase and in the metallic surface indicates that the origin of deposits over metallic surfaces are mainly due to the occurrence of the deposits precursors in liquid phase. These products could form dimers or trimers and form aggregates which precipitate and sediment due to the difference in polarity in comparison to the fuel phase. In the B0 sample, fossil diesel, these aggregates are kept in suspension since the oil-oil complex system formed after fuel aging does not present important differences in polarity between the aggregates and the supernatant media. On the other hand, biodiesel oil-oil complex system is unstable, the polarity between aggregates and solvent seems to be remarkable. This is in agreement with the work of Biernat *et al*. [27] that showed the increase of the polarity of oxidized FAME (at 95 °C, oxygen flow rate of 3 L/h) by using Electrochemical Impedance Spectroscopy (EIS). It is noteworthy that since B0 formulation contains only paraffins, naphtenes and aromatics, so, it does not contain any oxygenated specie prior to oxidation, whereas biodiesel samples have a great amount of methyl esters as well as unsaturated molecules, both of which are known to favor the oxidation process.[28] Furthermore, alkanes and esters will not form the same products after oxidation. [12] It seems that the products formed by B0 do not affect polarity in the same extend as the biodiesel products. This is

consistent with the observation made in real engine systems where oxidized B0 does not affect the injection system as much as an oxidized biodiesel sample. [29,30]

To better study the polarity of the system it would be interesting to study further the possible presence and impact of non-radical species that could probably play an important role in the phase separation, and so in the insoluble deposits formation. The impact of non-radical species over fuels degradation is poorly studied in the literature. This feature will be further investigated in a future work.

The adhesion of these aggregates to metallic surface seems to be related to other parameters as roughness, surface temperature and surface upper surfaces molecules affinity towards the oxygenated products present in the sediment. The study of these parameters is not in the scope of the present study and will be addressed in a future work.

## 5. CONCLUSION

Fuel oxidation process and the characterization of oxidation products were studied in order to identify the main levers to avoid deposits formation in engines. It was possible to observe by optical microscopy a complex emulsion on oxidized samples. The different phases observed after oxidation were studied, in particular the phase separation process, which could lead to the deposits observed in real systems. Turbiscan results show that the ranking for the demixing rate is B0<<< B10RME~B10SME~B30RME ~ B30SME, with B30 samples being the fastest ones to present the viscous sediment phase observed in oxidized samples. This order is the opposite in comparison to density and viscosity results. Therefore, there is no straightforward link between the weight of particulates and the deposits observed. Instead, it seems to be mainly related to the

polarity (e.g. oxygenates) content differences of both sediment and supernatant phases as shown by FTIR results. This feature can indicate that the deposits precursors are formed in liquid phase, and so, it is not primarily induced by the surface in contact with the fuel. This hypothesis is under investigation to understand the impact of non-radical species that could be formed during the fuels degradation process and that could probably play an important role in the phase separation. The insoluble deposits formation based on non-radical species reactions will be discussed in detail in our further work by using Electrochemical Impedance Spectroscopy (EIS). The understanding of sedimentation or phase separation process leading to deposits can be a key feature to develop strategies to prevent deposits formation in real engine systems.

## *References*


[1] Schaich KM. Lipid Oxidation: Theoretical Aspects. In: Shahidi F, editor. Bailey's Industrial Oil and Fat Products. Hoboken, NJ, USA: John Wiley & Sons, Inc; 2005.

[2] Pullen J, Saeed K. An overview of biodiesel oxidation stability. Renewable and Sustainable Energy Reviews 2012;16(8):5924–50. https://doi.org/10.1016/j.rser.2012.06.024.

[3] Jain S, Sharma MP. Stability of biodiesel and its blends: A review. Renewable and Sustainable Energy Reviews 2010;14(2):667–78. https://doi.org/10.1016/j.rser.2009.10.011.

[4] Richaud E, Djouani F, Fayolle B, Verdu J, Flaconneche B. New Insights in Polymer-Biofuels Interaction. Oil & Gas Science and Technology – Revue d'IFP Energies nouvelles 2013;70(2):317–33. https://doi.org/10.2516/ogst/2013151.

[5] Schaich KM. Thinking outside the classical chain reaction box of lipid oxidation. Lipid Technology 2012;24(3):55–8. https://doi.org/10.1002/lite.201200170.

[6] Frankel EN. Lipid oxidation: Mechanisms, products and biological significance. J Am Oil Chem Soc 1984;61(12):1908–17. https://doi.org/10.1007/BF02540830.

[7] Kuprowicz NJ, Zabarnick S, West ZJ, Ervin JS, Edwards T. Use of Measured Species Class Concentrations with Chemical Kinetic Modeling for the Prediction of Autoxidation and Deposition of Jet Fuels. Energy & Fuels 2007;21(2):530–44. https://doi.org/10.1021/ef060391o.

[8] Beate Richter, Svetlana Crusius, Ulrike Shcumann, Horst Harndorf. Characterization of Internal Deposits in common-rail injectors. Research Injector Systems. MTZ 2013.

[9] Barker J, Reid J, Snape C, Scurr D, Meredith W. Spectroscopic Studies of Internal Injector Deposits (IDID) Resulting from the Use of Non-Commercial Low Molecular Weight Polyisobutylenesuccinimide (PIBSI). SAE Int. J. Fuels Lubr. 2014;7(3):762–70. https://doi.org/10.4271/2014-01-2720.

[10] Fang HL, Mccormick RL. Spectroscopic Study of Biodiesel Degradation Pathways. SAE Technical Paper 2012(2006-01-3300):776–90.

[11] Alves-Fortunato M, Labaume J, Cologon P, Barré L. Biofuel Surrogate Oxidation: Insoluble Deposits Formation Studied by Small-Angle X-ray Scattering and Small Angle Neutron Scattering. Energy Fuels 2018. https://doi.org/10.1021/acs.energyfuels.8b02055.

[12] Bacha K, Ben-Amara A, Vannier A, Alves-Fortunato M, Nardin M. Oxidation Stability of Diesel/Biodiesel Fuels Measured by a PetroOxy Device and Characterization of Oxidation Products. Energy & Fuels 2015;vol. 29(7):pp. 4345–4355. https://doi.org/10.1021/acs.energyfuels.5b00450.

[13] Karl CHATELAIN. Etude de la stabilité à l'oxydation des carburants en phase liquide. Paris: ENSTA ParisTech; 2016.

[14] Fang HL, Mccormick RL. Spectroscopic Study of Biodiesel Degradation Pathways. SAE Technical Paper(2006-01-3300):pp. 776–790.

[15] Omori T, Tanaka A, Yamada K, Bunne S. Biodiesel Fuel Effects on Injection System and Establishment. SAE International 2011-28-0057.

[16] Maira Alves-Fortunato, Laurie Starck, Takuya Takahashi, Kazuhiro Ohmae, Yutaka Iida. Oxidation Stability of Diesel/Biodiesel Blends: Impact of Fuels Physical-Chemical Properties over Ageing During Storage and Accelerated Oxidation. In: SAE Technical Paper. SAE International; 2015.

[17] Kaombe DD, Lenes M, Toven K, Glomm WR. Turbiscan as a Tool for Studying the Phase Separation Tendency of Pyrolysis Oil. Energy Fuels 2013;27(3):1446–52. https://doi.org/10.1021/ef302121r.

[18] Formulation Smart Scientific Analysis. Turbiscan: The reference for stability analysis.

[19] kenza Bacha. Etude de l'Interaction entre le Carburant Diesel et les Composants du Système d'Injection Diesel. UNIVERSITE DE HAUTE ALSACE; 2015.

[20] Coates J. Interpretation of Infrared Spectra, A Practical Approach. In: Meyers RA, editor. Encyclopedia of analytical chemistry. Hoboken: John Wiley & Sons; 2006-.

[21] Nespeca MG, Hatanaka RR, Flumignan DL, Oliveira JE de. Rapid and Simultaneous Prediction of Eight Diesel Quality Parameters through ATR-FTIR Analysis. J Anal Methods Chem 2018;2018:1795624. https://doi.org/10.1155/2018/1795624.

[22] Chatelain K, Nicolle A, Ben Amara A, Catoire L, Starck L. Wide Range Experimental and Kinetic Modeling Study of Chain Length Impact on n -Alkanes Autoxidation. Energy Fuels 2016. https://doi.org/10.1021/acs.energyfuels.5b02470.

[23] Chatelain K, Nicolle A, Ben Amara A, Starck L, Catoire L. Structure–Reactivity Relationships in Fuel Stability: Experimental and Kinetic Modeling Study of Isoparaffin Autoxidation. Energy Fuels 2018;32(9):9415–26. https://doi.org/10.1021/acs.energyfuels.8b01379.

[24] Frankel EN. Lipid Oxidation: 2nd edition. Elsevier Science; 2014.

[25] Shahidi F (ed.). Bailey's Industrial Oil and Fat Products. Hoboken, NJ, USA: John Wiley & Sons, Inc; 2005.

[26] Zachary John West. STUDIES OF JET FUEL AUTOXIDATION CHEMISTRY: CATALYTIC HYDROPEROXIDE DECOMPOSITION & HIGH HEAT FLUX EFFECTS: UNIVERSITY OF DAYTON.

[27] Biernat K, Bocian P, Bukrejewski P, Noworyta KR. Application of the Impedance Spectroscopy as a New Tool for Studying Biodiesel Fuel Aging Processes. Energies 2019;12(4):738. https://doi.org/10.3390/en12040738.

[28] Kumar N. Oxidative stability of biodiesel: Causes, effects and prevention. Fuel 2017;190:328–50. https://doi.org/10.1016/j.fuel.2016.11.001.

[29] Alves Fortunato M, Lenglet F, Ben Amara A, Starck L. Are Internal Diesel Injector Deposits (IDID) Mainly Linked to Biofuel Chemical Composition or/and Engine Operation Condition? In: SAE International400 Commonwealth Drive, Warrendale, PA, United States; 2019.

[30] Ben Amara A, Lecointe B, Jeuland N, Takahashi T, IIda Y, Hashimoto H et al. Experimental Study of the Impact of Diesel/Biodiesel Blends Oxidation on the Fuel Injection System. SAE International Journal of Fuels and Lubricants 2014-2767:pp. 849–860. https://doi.org/10.4271/2014-01-2767.

## AUTHOR INFORMATION

### Corresponding Author

*Dr. Maira Alves Fortunato, e-mail: Maira.fortunato@ifpen.fr

### Author Contributions

The manuscript was written through contributions of all authors. All authors have given approval to the final version of the manuscript. ‡These authors contributed equally. (match statement to author names with a symbol

## ACKNOWLEDGMENT

The authors gratefully acknowledge the Transport Business Unit at IFPEN for the financial support, the staff of Chemistry and Applied Physical-Chemistry, Engine and Vehicles Systems and Physical Analysis at IFPEN for the experimental analysis.

## ABBREVIATIONS

| | |
|---|---|
| FAME | fatty acids methyl esters |
| FIS | fuel injection system |
| IDID | insoluble internal injector's deposits |
| RME | Rapeseed Methyl Ester |
| SME | Soy Methyl Ester |
| TAN | total acid number |
| B0 | Diesel without additives and without esters |
| B10 | B0 + 10%v/v of FAME |
| B30 | B0 + 30%v/v of FAME |

EIS Electrochemical Impedance Spectroscopy

## APPENDIX

| Parameter (EN14214) | Unit | B0 | RME | SME |
|---|---|---|---|---|
| Ester content | % m/m | --- | >99 | 98.8 |
| Density at 15°C | $Kg/m^3$ | 836.5 | 882.9 | 884.9 |
| Viscosity at 40°C | $mm^2/s$ | 2.52 | 4.402 | 4.133 |
| Flash Point | °C | --- | 176.5 | 168.5 |
| Oxidation Stability at 110°C | h | 51 | 8.1 | 6.0 |
| Acid Value | mg KOH/g | <0.01 | 0.083 | 0.194 |
| Iodine Value | --- | --- | 114 | 128 |
| linolenic acid methyl-ester | % m/m | --- | 10.4 | 7.2 |
| Water content | mg/kg | 0.006 | 272 | 98 |
| Metals I (Na+K) | mg/kg | --- | <1 | 1,2 |
| Metals II (Ca+Mg) | mg/kg | --- | <1 | <1 |